

High-Fidelity Model Order Reduction for Microgrids Stability Assessment

Petr Vorobev ¹, Member, IEEE, Po-Hsu Huang, Senior Member, IEEE, Mohamed Al Hosani ², Member, IEEE, James L. Kirtley, Jr., Life Fellow, IEEE, and Konstantin Turitsyn ³, Member, IEEE

Abstract—Proper modeling of inverter-based microgrids is crucial for accurate assessment of stability boundaries. It has been recently realized that the stability conditions for such microgrids are significantly different from those known for large-scale power systems. In particular, the network dynamics, despite its fast nature, appears to have major influence on stability of slower modes. While detailed models are available, they are both computationally expensive and not transparent enough to provide an insight into the instability mechanisms and factors. In this paper, a computationally efficient and accurate reduced-order model is proposed for modeling inverter-based microgrids. The developed model has a structure similar to quasi-stationary model and at the same time properly accounts for the effects of network dynamics. The main factors affecting microgrid stability are analyzed using the developed reduced-order model and shown to be unique for microgrids, having no direct analogy in large-scale power systems. Particularly, it has been discovered that the stability limits for the conventional droop-based system are determined by the ratio of inverter rating to network capacity, leading to a smaller stability region for microgrids with shorter lines. Finally, the results are verified with different models based on both frequency and time domain analyses.

Index Terms—Droop control, microgrids, reduced-order model, small-signal stability.

I. INTRODUCTION

THE advances in the renewable energy harvesting technologies and ever-growing affordability of electrical storage devices naturally lead to increased interest in microgrid development. Microgrids are expected not only to be an effective

solution for geographically remote areas, where the interconnection to the main power grid is infeasible, but also are considered as an improvement for conventional distribution networks during their disconnection from the feeding substation [1]–[3]. While in grid-connected mode, the simplest and most commonly used method of operation is to set renewable sources to maximum power output with the grid's interconnection taking responsibility for any power imbalances. With the increasing share of distributed generation and, more importantly, in the islanded mode of operation, there is a need for proper control of individual inverters power output [1], [4]. The problem of designing proper controls for microgrids has been the subject of intensive research in the last two decades. Comprehensive reviews [5]–[11] on the state-of-the-art in the field give an insight to the main approaches utilized for microgrid controls.

One of the first propositions for inverters connected to an AC grid were made more than two decades ago [12] with a droop control based on real power-frequency and reactive power-voltage control loops. These control methods were proposed to replicate conventional schemes utilized by large-scale central power generators for proper load sharing. The stability issue of microgrids operation was first recognized in [13] and [14] where small-signal stability analysis was carried out in a way similar to transmission grids. By looking at the mathematical and physical models utilized in these studies, there was no principle difference between microgrids and transmission grids and, hence, all principles of small-signal stability which are valid for large-scale power systems can be applied to microgrids. It was later realized that a high R/X ratio, which is typical for microgrids, can lead to considerable changes in microgrid stability regions [15] which was assigned mainly to distortion of a natural $P - \omega$ and $Q - V$ coupling which relies on predominantly inductive transmission lines. A number of approaches was proposed to deal with this issue specific to low voltage microgrids, most of them are based on the use of virtual impedance to restore $P - \omega$ and $Q - V$ coupling or the mixed droop method [16]–[21]. While the analysis and modeling of large-scale power systems has been thoroughly investigated in the literature with a certain number of modeling assumptions being already standard, there is far less experience and systematic studies of microgrids modeling with proper justification and validation. A natural question is whether the microgrids are similar to large-scale power systems or if there is a qualitative difference between them with certain phenomena being specific to microgrids.

Manuscript received October 21, 2016; revised March 8, 2017; accepted May 6, 2017. Date of publication May 23, 2017; date of current version December 20, 2017. This work was supported in part by the Masdar Institute of Science and Technology, Abu Dhabi, UAE, in part by MIT/Skoltech initiative, and in part by The Ministry of Education and Science of Russian Federation under Grant 14.615.21.0001, Grant identification code: RFMEFI61514X0001. Paper no. TPWRS-01581-2016. (Corresponding author: Petr Vorobev.)

P. Vorobev is with the Department of Mechanical Engineering, Massachusetts Institute of Technology, Cambridge, MA 02139 USA, and also with the Skolkovo Institute of Science and Technology, Moscow 143026, Russia (e-mail: petrvaro@mit.edu).

P.-H. Huang and J. L. Kirtley, Jr. are with the Department of Electrical and Computer Engineering, Massachusetts Institute of Technology, Cambridge, MA 02139 USA (e-mail: pohsu@mit.edu; kirtley@mit.edu).

M. Al Hosani is with the Department of Electrical Engineering and Computer Science, Khalifa University of Science and Technology, Masdar Institute, Abu Dhabi 54224, UAE (e-mail: mohalhosani@masdar.ac.ae).

K. Turitsyn is with the Department of Mechanical Engineering, Massachusetts Institute of Technology, Cambridge, MA 02139 USA (e-mail: turitsyn@mit.edu).

Color versions of one or more of the figures in this paper are available online at <http://ieeexplore.ieee.org>.

Digital Object Identifier 10.1109/TPWRS.2017.2707400

Modeling of microgrids, as any other engineering system, relies heavily on the appropriate choice of simplifications. With respect to small-signal stability analysis, the main question is whether a particular model reduction technique can give qualitatively incorrect results (i.e., predicting stability while in reality the system is unstable or vice-versa). A detailed model for stability assessment of microgrids was developed in [22] considering all internal states of an inverter as well as network dynamics. Since then, this model was extensively used in literature for stability assessment of microgrids with different configurations and control settings. While detailed models are the most reliable in stability assessment, they suffer from certain drawbacks such as: a) detailed models can easily become very complex and computationally demanding with the increase in the system size as well as with the addition of certain components with non-trivial dynamic properties; b) it is very difficult to get an insight into the key factors influencing stability, thus they are hardly used as guidelines for development of new control techniques or provide simple ways of stability enhancement; c) detailed models require more accuracy in actual realization which increases the chance of modeling errors and incorrect predictions. Thus, there is a great demand for reliable and simple enough reduced-order models which not only decrease the computational efforts but also provide the insight into physical origins of instability. Moreover, such reduced-order models enable a framework allowing for development of more advanced stability assessment methods as were recently presented for quasi-stationary representation [23]–[25].

The first attempts to model microgrids in a simple way were made following the experience from large-scale power systems neglecting the network dynamics [12]–[14]. This approach seemed reasonable since there exist a distinct time-scale separation between different degrees of freedom in inverter-based microgrids with only the slowest modes being of interest from stability point of view [22]. Timescales of network dynamics are determined by electromagnetic transient time constants which are very small (of the order of few milliseconds) for resistive microgrids (X/R ratio is around unity), much smaller than the characteristic timescales of power controllers. The timescales associated with the inverter internal controls (current and voltage controllers) are even smaller. Recently a number of papers approached model order reduction based on this time-scale separation where quasi-stationary approximation was applied on a detailed model with proper choice of degrees of freedom to omit [26]–[28].

Unlike in large-scale power systems, where a distinct separation of time-scales allows for a straight model order reduction, in microgrids certain fast modes (mostly electromagnetic) can significantly influence the dynamics of slow ones, which was originally assigned to the fact that the effective “inertia” of inverter dynamics is small. One of the first, to our knowledge, reduced-order models that captures the effects of fast network dynamics was developed in [29] where the network effect on system dynamics was incorporated by a certain perturbation method. The importance of network dynamics despite its very fast nature was pointed out in [30] where a similar perturbation approach was used. In [28], the inadequacy of oversimplified

models was further emphasized where it was explicitly shown that in certain situations, the full-order model predicts instability while the reduced-order (Kuramoto’s) model predicts stability for a wide range of parameters. A model reduction technique based on singular perturbation theory was introduced in [31] allowing for proper exclusion of fast degrees of freedom, which is based on the formal summation of multiple orders of expansion in powers of small parameters (timescale ratio) as opposed to quasi-stationary approximation leaving just zero-order terms.

It is clear from the literature that a simple timescale ratio could be insufficient for justification of exclusion of certain degrees of freedom - even very fast states can still influence the slow modes. On the other hand, the strong natural time-scale separation (for example, noted in [22]) existing in microgrids should allow for proper model order reduction. Ideally, one would think about getting a reduced-order model containing only the slowest modes of interest and allowing for accurate stability prediction. Along with accuracy and computational efficiency, the reduced-order model should also allow for physical interpretation of the instability mechanisms and identification of the main factors affecting stability limits.

This paper concentrates on systematic approach for development of such high-fidelity reduced-order models with special emphasis on the physical mechanisms of fast variables participation in the dynamics of slow modes. The obtained reduced-order model will be used to draw a number of practically important conclusions about the trends in microgrids stability. The key contributions of this paper are as follow:

- 1) A reliable and concise reduced-order model for microgrids is developed allowing for accurate stability assessment and uncovering the main factors affecting microgrids stability. It has been explicitly shown that the obtained stability conditions are unique for microgrids and can not be directly explained using the example of large-scale power system.
- 2) The influence of fast degrees of freedom on system dynamics is properly quantified and the reasons for inadequacy of quasi-stationary (with respect to network dynamics) approximation are given. We demonstrate that it is the network dynamics that plays the main role in stability violation and neglecting it leads to overly optimistic stability regions.
- 3) Generalization of the proposed method to arbitrary sets of slow and fast degrees of freedom is presented and explicit form of reduced-order equations for microgrids with multiple inverters and arbitrary network structure is derived. The resulting equations contain dynamics of only local variables and are mathematically similar to coupled oscillators which allows for potential application of advanced stability assessment methods.

The rest of the paper is organized as follows: in Section II, the problem is formulated based on a two-bus example and the reduced-order model is derived with explicit demonstration of the role of fast degrees of freedom on the dynamics of slow modes. The proposed model is then compared to the quasi-stationary model and a physical explanation of instability mechanism is provided as well as phenomena specific to

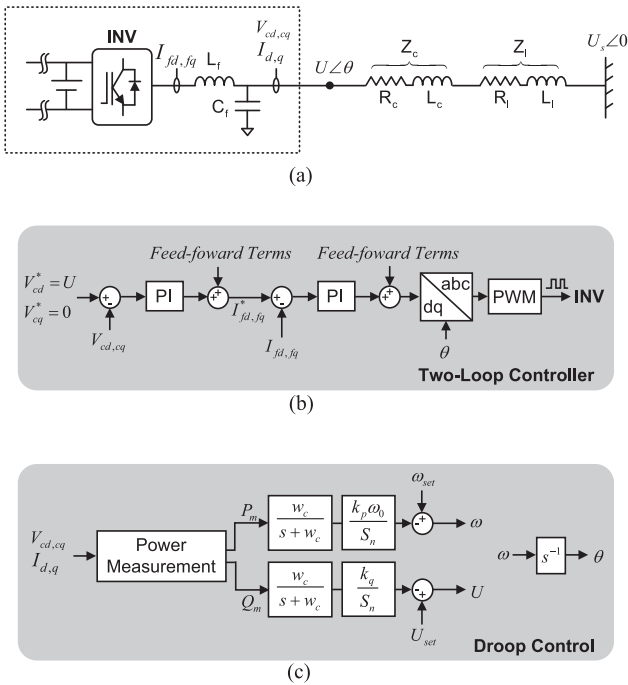


Fig. 1. The two-bus system under study. (a) Network configuration. (b) Two-loop controller. (c) Droop controller.

microgrids are discussed. Section III gives a formal mathematical formulation of the problem and presents a general way to perform model order reduction for arbitrary systems. Section IV describes an application of the mathematical model to microgrids with arbitrary network structure. Section V provides the results of direct numerical simulations based on the proposed reduced-order model and presents explicit numerical comparisons for different models under investigation. Finally, conclusions are drawn in Section VI.

II. TWO-BUS MODEL

In this section, the microgrid stability problem that motivates this study is illustrated using a simple two-bus system shown in Fig. 1(a). We follow the standard two-loop control system comprised of the inner current loop and outer voltage loop with feed-forward compensations [22], as shown in Fig. 1(b). In general, the inner loop is designed to be much faster than the outer one, allowing independent tuning of the inner and outer control gains. While preventing over-current references fed to the current controller, the overall synthesized control achieves regulation of the filter capacitor voltage based on the given voltage reference, $V_{cd}^* = U$, $V_{cq}^* = 0$ so that the LC filter can also be considered as a part of this control scheme (since the tuning of both inner and outer loops takes into account LC filter parameters). Meanwhile, the integral of the frequency reference is used for generating the pulsewidth-modulated (PWM) signal. Finally, the frequency/voltage references are supplied by the droop control as shown in Fig. 1(c).

Therefore, the following setting based on per-unit representation will be utilized in this section. A single inverter unit with

nominal power S_n in p.u. is connected to an infinite bus (fixed voltage U_s and frequency ω_0) by a coupling impedance with resistance R_c and inductance L_c and a line with resistance R_l and inductance L_l . The inverter operates in a droop-controlled mode 1(c), such that the equilibrium frequency is related to the output real power while the inverter terminal voltage is related to the reactive power according to the relations [22]:

$$\omega = \omega_{\text{set}} - \frac{k_p \omega_0}{S_n} P, \quad U = U_{\text{set}} - \frac{k_q}{S_n} Q \quad (1)$$

where $S_n = S_{\text{inv}}/S_b$ denotes the inverter rating in respect to the base power S_b , while ω_{set} and U_{set} are the set points of frequency and voltage controllers, respectively. It should be noticed that we consider both ω and ω_0 to be measured in *rad/s*. The variables P and Q in (1) are the active and reactive power filtered by means of passing the measured instantaneous values (denoted as P_m and Q_m) through a low-pass filter:

$$P = \frac{1}{1 + \tau s} P_m, \quad Q = \frac{1}{1 + \tau s} Q_m \quad (2)$$

where $\tau = \omega_c^{-1}$ is the power controller filter time (or the inverse of the filter cut-off frequency). The values of k_p and k_q are the per-unit frequency and voltage droop gains, respectively. It should be noted that the droop gains k_p and k_q are normalized to the individual inverter rating S_n (which might be different for different inverters in the system) thus representing a natural relative gain of each inverter. Typically, the values of k_p and k_q are set within 0.5% – 3% [22].

For small-signal stability analysis of an AC system operating at equilibrium with a certain frequency ω_0 , it is convenient to employ the following dynamic representation:

$$v(t) = \text{Re}[V(t)e^{j\omega_0 t}]; \quad i(t) = \text{Re}[I(t)e^{j\omega_0 t}], \quad (3)$$

where the complex amplitudes $V(t)$ and $I(t)$ can be arbitrary (not necessarily slowly varying) functions of time. In the case of grid-connected inverter, the equilibrium frequency ω_0 coincides with the grid frequency. The index 0 is used throughout the paper to denote the equilibrium values of corresponding variables. It should be noted that (3) represent a mathematical change of functions and do not introduce any approximation to dynamic equations - i.e., no restrictions are imposed on how fast the phasors $V(t)$ and $I(t)$ can change. Similar representation is used in [29] and [30].

The rest of this section is organized as follows. First, an initial model for a droop-controlled inverter that includes both fast and slow variables is presented. Then, a simple model order reduction technique based on the quasi-stationary approximation is illustrated. Following we introduce a proper model order reduction procedure explicitly demonstrating the failure of the quasi-stationary model and uncovering the physical mechanisms of fast degrees of freedom participation in dynamics of slow modes. Then, an explicit comparison with large-scale power systems is carried out to show why the approaches used for the latter fail to properly describe microgrids.

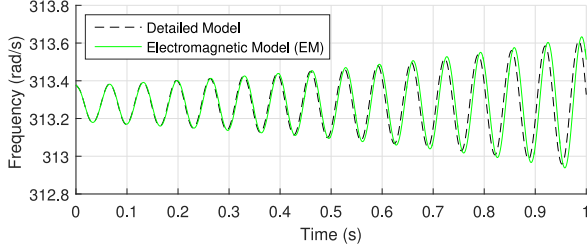


Fig. 2. Time-domain simulations using electromagnetic 5th-order vs detailed inverter model from [22].

A. Electromagnetic 5th-Order Model

In our initial model, the inverter with its LC filter is considered as an effective voltage source governed by the slower droop control. Following this model, $U\angle\theta$ is used to represent the inverter effective terminal voltage and phase angle after the LC filters. This allows us to effectively describe the system using only inverter terminal states (angle, frequency and voltage) and line currents as dynamic variables, bypassing all the inverter internal states.

Therefore, for the two-bus system in Fig. 1, we start from a 5th-order electromagnetic (EM) model with three states related to the inverter (angle, frequency and voltage) and two states - to the line (two components of current phasor). The per-unit equations describing such a model in dq reference frame are:

$$\frac{d\theta}{dt} = \omega - \omega_0 \quad (4)$$

$$\tau \frac{d\omega}{dt} = \omega_{\text{set}} - \omega - \frac{k_p \omega_0}{S_n} P_m \quad (5)$$

$$\tau \frac{dU}{dt} = U_{\text{set}} - U - \frac{k_q}{S_n} Q_m \quad (6)$$

$$L \frac{dI_d}{dt} = U \cos \theta - U_s - RI_d + \omega_0 LI_q \quad (7)$$

$$L \frac{dI_q}{dt} = U \sin \theta - RI_q - \omega_0 LI_d \quad (8)$$

Here, (5) and (6) represent the dynamics of the terminal voltage and frequency, and incorporate the low-pass filters of the inverter power control system characterized by the bandwidth $w_c = \tau^{-1}$. (7) and (8) model the electromagnetic dynamics of the complex current $I(t)$ defined in (3). The values $L = L_c + L_l$ and $R = R_c + R_l$ are the aggregate inductance and resistance of connection, respectively, as seen by the inverter terminal. This model can be validated by directly running time-domain simulations versus the detailed inverter model [22] containing all the inverter internal states. The result of such simulations for operation slightly outside stability region is shown in Fig. 2, which clearly indicates the validity of representation (4)–(8).

With a typical low voltage microgrid in mind, the system parameters shown in Table I will be used for our further calculations [27]. For the described system, the characteristic electromagnetic time (assuming a 1 km length of connecting line) is $L/R \approx 3.1$ ms, below both the base cycle period of $2\pi\omega_0^{-1} = 20$ ms and the characteristic timescale of droop con-

trols ($\tau \approx 31.8$ ms). Only the slowest modes associated with voltage and angular dynamics are of interest from the stability point of view [22], [32]. The strong time-scale separation in such a system between these slow modes and current dynamics is usually used as a justification for model order reduction. Indeed, given the fast electromagnetic transients, one may assume that the currents I_d, I_q always remain close to their quasi-stationary values derived from Kirchhoff's laws. Formally, this procedure is equivalent to neglecting the derivative terms in the left-hand side of (7) and (8). This approximation is universally accepted for small-signal stability analysis in traditional power systems. However, in the following discussion, the inappropriateness of using such an approximation is to be demonstrated and investigated. Also, a discussion on the strong effect of electromagnetic transients on microgrid stability will be carried out with the introduction of the proposed order reduction procedure for accurate stability assessment.

B. Conventional 3rd-Order Model

As discussed above within a traditional quasi-stationary approximation (also called zero's order approximation), one neglects the effect of electromagnetic transients which formally corresponds to setting the derivative terms in the left-hand side of (7) and (8) to zero. The line currents become algebraic functions of terminal voltage and phase:

$$I^0 = (R + j\omega_0 L)^{-1} (Ue^{j\theta} - U_s) \quad (9)$$

where subscript $\{0\}$ denotes the equilibrium frequency while the superscript $\{0\}$ attached to current phasor denotes that the latter is calculated at zero's order approximation. Then, the following expressions for active and reactive power in zero's order approximation are obtained from (9):

$$P_m^0 = B \sin \theta + G(U/U_s - \cos \theta) \quad (10)$$

$$Q_m^0 = B(U/U_s - \cos \theta) - G \sin \theta \quad (11)$$

where $B = UU_s \omega_0 L / (R^2 + \omega_0^2 L^2)$ and $G = UU_s R / (R^2 + \omega_0^2 L^2)$. The small-signal stability of the base operating point will be assessed by introducing deviations of the angle $\delta\theta$ and normalized voltage $\delta\rho = \delta U/U$ from their equilibrium values. Then, the linearized equations can be rewritten in the following form:

$$\lambda_p \tau \ddot{\delta\theta} + \lambda_p \dot{\delta\theta} + \frac{\partial P_m^0}{\partial \theta} \delta\theta + \frac{\partial P_m^0}{\partial \rho} \delta\rho = 0 \quad (12a)$$

$$\lambda_q \tau \dot{\delta\rho} + \lambda_q \delta\rho + \frac{\partial Q_m^0}{\partial \theta} \delta\theta + \frac{\partial Q_m^0}{\partial \rho} \delta\rho = 0 \quad (12b)$$

where $\lambda_p = S_n (\omega_0 k_p)^{-1}$, $\lambda_q = S_n (k_q)^{-1}$, $\tau = w_c^{-1}$, and $\omega_0 = 100\pi$. It should be noted that $\delta\rho$, $\delta\theta$, U , U_s , U_0 , S_n , G , and B are all dimensionless in this expression.

Next, we assume that the operating point itself corresponds to small equilibrium values of angle, $\theta \approx 0$, and voltage is close to nominal value, $U \approx U_0 \approx U_s = 1$ pu. For the typical parameters used in this paper, this assumption is well justified, as the typical angle difference and relative voltage deviations are of the order $\sim 10^{-2}$ [28], [30]. Extension of the analysis to

heavily loaded regimes is straightforward but bulky and will be presented in subsequent publications. Under these assumptions, the system in (12) reduces to a concise form:

$$\lambda_p \tau \ddot{\delta\theta} + \lambda_p \dot{\delta\theta} + B\delta\theta + G\delta\rho = 0 \quad (13a)$$

$$\lambda_q \tau \dot{\delta\rho} + (\lambda_q + B)\delta\rho - G\delta\theta = 0 \quad (13b)$$

The form of equations in (13) indicate that in the absence of conductance, the dynamics of the angle and voltage deviations become uncoupled and the system is always stable. Active resistance introduces an effective positive feedback to the system and may lead to the loss of stability. The detrimental effect of the conductance on stability can be illustrated using the following informal argument based on the multi-time-scale expansion approach utilized in this work. Equation (13b) implies that the voltage deviation follows the deviation of the angle with some delay:

$$\delta\rho(t) = \frac{G}{\lambda_q \tau} \int_0^\infty \exp\left[-\frac{(\lambda_q + B)T}{\lambda_q \tau}\right] \delta\theta(t - T) dT, \quad (14)$$

When dynamics of $\delta\theta$ is slow enough, the effect of delay can be approximated as

$$\delta\rho(t) \approx \frac{G}{\lambda_q + B} \delta\theta(t) - \frac{\lambda_q \tau G}{(\lambda_q + B)^2} \dot{\delta\theta}(t) \quad (15)$$

This expansion can be obtained by applying a first-order Taylor expansion to $\delta\theta(t - T)$ in (14) and neglecting the contribution of higher-order derivatives of $\delta\theta$. Plugging expression (15) back in (13a), the following approximation is obtained:

$$\lambda_p \tau \ddot{\delta\theta} + \left[\lambda_p - \frac{\lambda_q \tau G^2}{(\lambda_q + B)^2} \right] \dot{\delta\theta} + \left(B + \frac{G^2}{\lambda_q + B} \right) \delta\theta = 0 \quad (16)$$

The above approximation illustrates the effect of delay on the system stability. For high conductance values, the effective damping coefficient in front of $\dot{\delta\theta}$ can become negative which results into instability. This can happen for any arbitrary ratio of timescales of the system modes, since the characteristic timescale is not the only relevant parameter but rather it's the product with the corresponding gain. Assuming $S_n = 1$, the system would remain stable whenever k_p satisfies

$$k_p < \frac{(1 + k_q B)^2}{\omega_0 k_q \tau G} \quad (17)$$

This argument is not entirely rigorous since dynamics of $\delta\theta$ is not necessarily slower than dynamics of $\delta\rho$, although the resulting condition on k_p is reasonably accurate and highlights the importance of delays. However, a similar procedure can be applied to account for delays caused by the line inductance which will be shown to be important for microgrids. In the case of electromagnetic delays in lines the application of multi-time-scale expansion is well justified since the electromagnetic delay time is much smaller than the typical time-scale of voltage and angle dynamics.

C. High-Fidelity 3rd-Order Model

As discussed above, the conventional (quasistationery) 3rd-order model becomes inappropriate for microgrids because elec-

tromagnetic transients start to play a critical role in the onset of instability despite their short timescale (the inappropriateness of such a model was explicitly discussed in [30] and [28]). Mathematically, these electromagnetic transients manifest themselves in the derivative terms of the left hand side of (7) and (8) which cannot be fully neglected. Nevertheless, it is possible to account for these transients by deriving an effective 3rd-order model which will allow for accurate stability assessment. We will refer to this model as ‘‘high-fidelity model’’. In Laplace domain, (7) and (8) can be explicitly solved for I_d and I_q via a first-order transfer function

$$I = \frac{U e^{j\theta} - U_s}{R + j\omega_0 L + sL} = \frac{I^0}{1 + sL/(R + j\omega_0 L)}. \quad (18)$$

Whenever the goal is to derive an equivalent reduced-order model capturing the dynamics of slow modes, it is reasonable to assume that $|sL/(R + j\omega_0 L)| \ll 1$ holds for modes that evolve on the time-scales slower than the electromagnetic time L/R . In this case, one can perform Taylor series expansion on (18) to get

$$I \approx I^0 - \frac{Ls}{R + j\omega_0 L} I^0. \quad (19)$$

Returning back to the time domain, (19) can be rewritten as

$$I \approx I^0 - \frac{L}{R + j\omega_0 L} \frac{dI^0}{dt} \quad (20)$$

Then, the approximate values of P_m and Q_m are obtained as follows (detailed derivation is provided in Appendix A):

$$P_m \approx P_m^0 - G' \dot{\rho} - B' \dot{\theta} \quad (21)$$

$$Q_m \approx Q_m^0 - B' \dot{\rho} + G' \dot{\theta}, \quad (22)$$

where G' and B' are given by

$$G' = \frac{L(R^2 - \omega_0^2 L^2)}{(R^2 + \omega_0^2 L^2)^2}; \quad B' = \frac{2\omega_0 RL^2}{(R^2 + \omega_0^2 L^2)^2}. \quad (23)$$

Hence, the real and reactive powers now depend not only on the voltage magnitude and angle values, but also on their rates of change. In general, the terms with derivatives in (21) are small compared to the quasi-stationary contribution from P_m^0 and Q_m^0 , which justifies the expansion; however, these terms will contribute to the corresponding derivative terms in the dynamic equations. The equations for angular and voltage dynamics, instead of (13) now become:

$$\lambda_p \tau \ddot{\delta\theta} + (\lambda_p - B') \dot{\delta\theta} + B\delta\theta + G\delta\rho - G' \dot{\delta\rho} = 0 \quad (24a)$$

$$(\lambda_q \tau - B') \dot{\delta\rho} + (\lambda_q + B)\delta\rho - G\delta\theta + G' \dot{\delta\theta} = 0 \quad (24b)$$

These equations can be analyzed in a similar way to obtain a generalized version of (17). However, some important straightforward qualitative conclusions can be made from the basic structure of (24). The natural negative feedback terms for $\dot{\delta\theta}$ and $\dot{\delta\rho}$ can change sign when the corresponding droop coefficients are increased (meaning the decrease in λ_p and/or λ_q) - the effect is exclusively due to the network dynamics and was not present in the conventional 3rd-order model. Thus, a simple set of stability conditions can be obtained by requiring these terms

in front of the first derivatives to be positive, i.e., $(\lambda_p - B') > 0$ and $(\lambda_q \tau - B') > 0$ which upon substitution of λ_p , λ_q and B' turns into:

$$k_p < S_n \frac{(R^2 + X^2)^2}{2RX^2}; \quad k_q < \tau \omega_0 S_n \frac{(R^2 + X^2)^2}{2RX^2}, \quad (25)$$

where $X = \omega_0 L$. It is important to emphasize that the small timescale of the electromagnetic phenomena L/R cannot be used as a reliable indicator of the insignificance of the network dynamics. Specifically, even if the second term in (20) is small compared to the first (which is actually the case and is the justification for expansion), this term contributes to a different order of derivative in the dynamic equation (the derivative terms in (24)), so that the true conditions on the insignificance of network dynamics are $B' \ll \lambda_p$ and $B' \ll \tau \lambda_q$ with the former being usually stronger. To avoid confusion, we note that relations (25) do not represent the exact stability criteria but rather give a general estimation of the small-signal stability boundary in terms of frequency and voltage droop coefficients and are very good for demonstrating the key factors affecting stability as well as validity of the model. The general observations from (25) are:

- 1) Decrease in the line reactances and resistances (i.e., improving the connection to the grid) has a deteriorating effect on stability.
- 2) Decreasing the inverter rating (i.e., connecting smaller inverter with the same relative settings and same coupling impedance) reduces stability region.
- 3) Increasing the inverter control filtering time affects the small-signal stability boundary mainly with respect to the voltage droop gain.

These general stability properties have no analogy on the level of large-scale power systems. In fact, the first two are exactly the opposite of what has been well known for transmission grids where improving the network connections always has a positive effect on stability [33]. Below we give a more detailed discussion of each of these properties verified by the corresponding direct numerical simulations based on the initial EM model.

A comparison of three different models (the 5th-order EM model presented in (4)–(8), the conventional 3rd-order model and the proposed high-fidelity 3rd-order model) is presented in Fig. 3 with the predicted stable region being to the left of the corresponding curve. The droop coefficients relative to inverter rating are used as relevant parameters for stability regions representation. It is obvious that the electromagnetic transients play important role in stability violation and that the conventional 3rd-order model is highly inappropriate for stability assessment since it predicts a substantially larger stability region than the other two models (as was pointed in [28], this simple oscillator-type model predicts stable operation for almost any realistic microgrid configuration). It is important to note that according to (24a) and (24b), the electromagnetic modes start to be relatively unimportant if one considers only sufficiently small values of droop coefficients corresponding to $\lambda_p \gg B'$ and $\lambda_q \gg B'$ thus being far away from the stability boundary. Any dynamic simulations in this region using either of the models (quasi-stationary 3rd-order, high-fidelity 3rd-order or 5th-order EM) will give very similar results. This is an important observation,

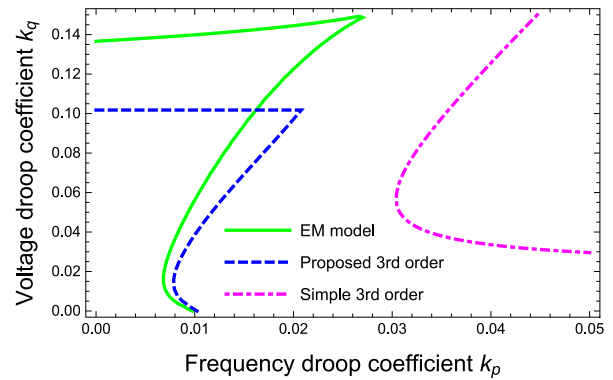


Fig. 3. Comparison of stability regions predicted by three different models (EM model refers to the electromagnetic 5th-order model).

since it states that dynamic simulations for a certain microgrid setting can be misleading in terms of the model verification - one has to specifically look for stability boundary predicted by the model in order to test its validity. The numerical simulations confirming this statement are provided in Section V.

D. Effect of Line Impedance

The numerical simulation using a 10 kVA inverter connected to a grid through a line with parameters given in Table I produces a stability boundary of $k_p \sim 0.5\text{--}2\%$ and $k_q \sim 2\text{--}25\%$ depending on the connecting line length and filter time constant. The result is specific to microgrids and has no analogy to large-scale transmission grids, and can be understood in the following way. Let us use a term “line rating” to refer to a quantity $S_l \sim V^2/Z_l$ which represents an order of magnitude of power that can be transmitted over a line until the formal violation of angular and/or voltage stability. Let us assume that the line resistance and reactance are of the same order (which is true for low-voltage grids under consideration). Then, according to (25), the maximum value of relative frequency droop coefficient is simply the ratio of inverter rating to line rating. For the parameters under consideration, the line rating is of the order of several hundreds of kVA (for a 1 km line with parameters from Table I, the rating is around 750 kVA) which is two orders of magnitude higher than the typical inverter rating. Contrary to large transmission systems, where power flows are mostly limited by voltage drop and angular stability, the main limitation in microgrids is the heating overcurrent limit of conductors. Consequently, microgrids typically operate in a region of very small values of inverter angles θ (or, more precisely, angle differences), this fact was also noted in [30]. For large transmission systems, generator ratings are usually of the same order as line ratings (mainly due to machine internal inductances) and, hence, the formal stability limit for machine is around $k_p \sim 100\%$ which is never used in practice for other reasons.

For the microgrid network under consideration, on the contrary, a narrow stability boundary is shown - around $k_p \sim 1\%$ which is roughly the ratio of inverter rating to “line rating”. In fact, by assuming that the X/R ratio of the connection is fixed

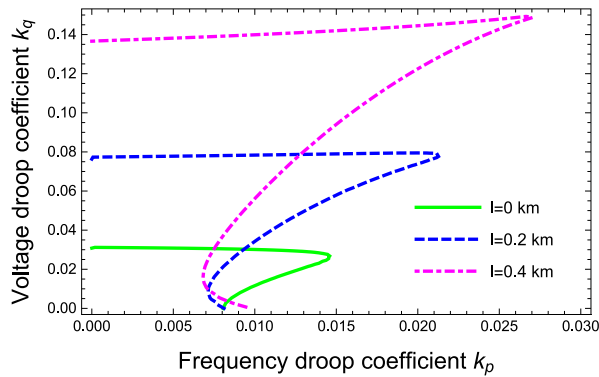


Fig. 4. Stability regions for different lengths of connection line.

(although it is slightly distorted by the presence of coupling inductance which can have an X/R different from that of the network), then the term B' is simply inversely proportional to connection length, so is the maximum frequency droop coefficient. It is, therefore, the absence of large impedance which makes the inverter-based microgrids completely different from large-scale power systems and synchronous machine-based grids in terms of stability. A synchronous machine connected to a low-voltage grid also does not exhibit instabilities at such low values of frequency droop, despite the fact that such machines can formally be described by equations similar to (5)-(8), since machines normally have large internal reactance $X' \sim 0.2 - 0.5$ which makes the term B' smaller. From this point of view, one can also give a rather simple explanation why the electromagnetic transients are not important for large-scale power systems and even for small-scale synchronous machines (despite the larger timescale of these transients compared to inverter-based microgrids due to more inductive impedances of machines). Specifically, the effect of electromagnetic transients is negligible if the B' term in (24a) and (24b) is much smaller than λ_p . The former has an order of magnitude similar to the inverse impedance in p.u. which for large-scale power grids is around unity, while the latter is the inverse frequency droop - at least one order of magnitude higher. Moreover, these effects are not directly related to the generator time constant or, in the case of inverter, the filter time constant τ (while the constant τ does affect stability region (Fig. 6), it has no direct connection with the validity of quasi-stationary approximation), which is often mentioned as the main reason for the importance of network dynamics for microgrids. It is rather the small per-unit values of network characteristic impedances that makes it necessary to consider electromagnetic transients.

The influence of different connecting line lengths on stability is illustrated in Fig. 4 with the blue curve corresponding to direct inverter connection and the effective line impedance is only due to the internal coupling impedance. As noted in Fig. 4, the increase in the connecting line impedance tends to increase the overall stability region especially in terms of voltage droop coefficient. While there is no strict monotonic dependence of the maximum frequency droop coefficient on the connecting line lengths, there seems to exist a robust stability region corresponding to the lower left corner of Fig. 4 which is due to

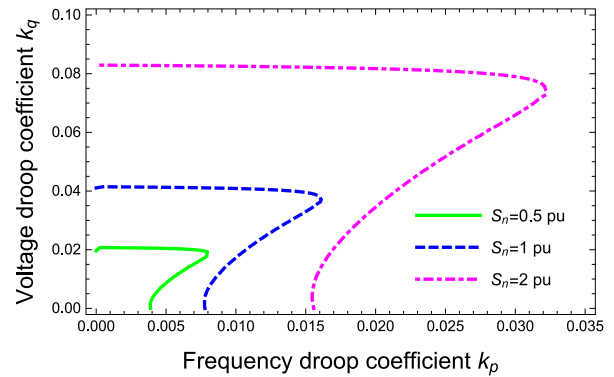


Fig. 5. Stability regions for different inverter rating values, 1 pu = 10 kVA.

the minimum coupling impedance always being present in the system. It is important to note that the stability region can be expanded either by using lines with greater impedance (especially with large reactance) or by adding substantial amount of virtual impedance. In this case, equations (24a) and (24b) as well as the relations in (25) can give a key on the proper sizing of this virtual impedance for a given set of target droop coefficients.

Let us also give a rather simple physical interpretation to the instability mechanism in terms of time delays in network current. One can think about the exact current $i(t)$ being retarded with respect to quasi-stationary value i^0 by the characteristic electromagnetic time L/R which decreases as R increases, such that one might expect the quasi-stationary approximation (conventional 3rd-order model) to work better with decreasing X/R ratio. However, it is not the delay itself, but rather the product of delay and gain that determines the overall effect on stability. While the delay time is inversely proportional to R , the corresponding gain, which is determined by the $1/B'$ term in (24a) and (24b), is proportional to R^2 so that the quasi-stationary approximation becomes less applicable for resistive lines despite the decrease in electromagnetic delay times.

E. Inverter Rating and Power Filter Time Constants

According to (25), the inverter rating has major influence on the stability boundary in terms of the relative voltage and frequency droop coefficients. In fact, one can refer directly to (24a) and (24b) to infer the role of inverter rating. Stability regions in the space of relative droop coefficients for inverters of ratings 5, 10 and 20 KVA, respectively, are illustrated in Fig. 5. The stability criteria for small inverters are becoming stricter with the acceptable values of relative frequency droop k_p becoming less than 0.5%. An important practical conclusion from this observation is that connecting few smaller inverters instead of a single larger one while keeping the same relative settings for droop controls can lead the system to instability. To avoid any confusion, it should be pointed out that if one sets the absolute droop coefficients in $(rad/s)/W$ and V/VAR , respectively, the stability is not affected by the inverter rating. It is however reasonable to consider the droop settings in relative units, similar to the way it is done in large-scale power systems.

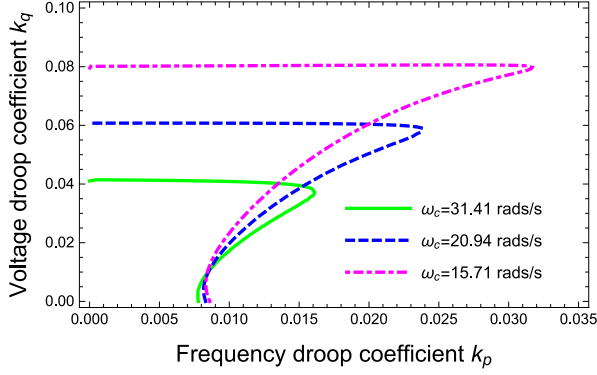


Fig. 6. Stability regions for different power filter cut-off frequencies.

Equation (25) also allows for drawing some general conclusions about the influence of the power filters cut-off frequency on stability regions. The filtering time constant plays a role of “inertia” and is considered to be one of the major factors influencing stability. Equation (25) suggests that the filtering time constant has the most affect on the small-signal stability region with respect to the voltage droop coefficient value, which is confirmed by direct numerical simulations given in Fig. 6. Increasing the inverter filter time constant significantly broadens the stability region; however, extension to the larger values of frequency droop is only possible if the voltage droop is varied correspondingly (as seen in Fig. 6).

F. Virtual Impedance Methods

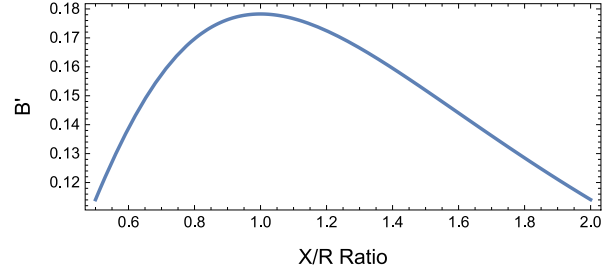
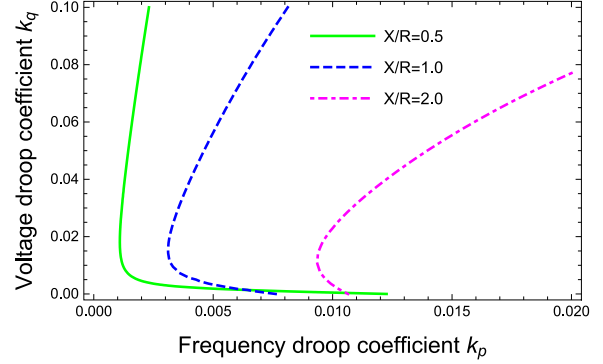
It has been shown previously that the stability region of the droop-controlled inverter system is constrained mainly due to the presence of B' term in (24a) and (24b). This, so-called, transient susceptance B' becomes larger as a result of stronger coupling between the inverter and the grid. In [17], it has been indicated that installation of additional coupling inductors is recommended for enhancing the stability, however, such a bulky inductor is not always desirable. Thus, several research works have proposed the concept of virtual impedances, virtual inductances or virtual synchronous generators [16], [17], [34], [35].

As mentioned previously, we follow a standard two-loop control concept consisting of inner current and outer voltage loops. In general, the response of voltage regulation is fast enough to allow synthesizing different dynamic behaviors. Therefore, to mimic the virtual impedance, additional terms that react to the output currents are added for emulating the inductive dynamics. That is, the modified reference voltages in Fig. 1 are given by the following forms:

$$V_{cd}^* = U + X_m I_q - \frac{s\omega_f L_m}{s + \omega_f} I_d \quad (26a)$$

$$V_{cq}^* = 0 - X_m I_d - \frac{s\omega_f L_m}{s + \omega_f} I_q \quad (26b)$$

where $X_m = \omega_0 L_m$ denotes the virtual reactance, ω_f is the cut-off frequency of the high-pass filter, $V_{cd,cq}^*$ are the modified


 Fig. 7. Variation of B' with respect to X/R ratio.

 Fig. 8. Stability regions for different X/R ratios.

reference voltages for the two-loop control scheme, and $I_{d,q}$ are the output currents in dq axis. One can note that the above mentioned control scheme may have different equivalent forms that result in similar dynamic behavior, and here we follow a configuration similar to one proposed in [34]. Details of particular implementation are beyond the scope of this paper.

With the deployment of virtual impedances/inductances, expansion of the stability region can be explained by considering the change of corresponding $B' = 2RX^2/(\omega_0 Z^4)$ value, whose variation with X/R ratio is shown in Fig. 7, where $X = \omega_0(L_m + L_l + L_c)$ and $R = R_l + R_c$. Thus, (24a) and (24b) give a guideline for proper sizing of the virtual impedance if achieving stability for certain droop coefficients is targeted. It can be seen that the value of B' peaks when $X/R = 1$, implying that bidirectional perturbation of X/R away from unity allows expansion in stability range of k_p assuming that k_q is sufficiently small. That is, when the interaction between droop and voltage modes is weak (low k_q), a negative damping coefficient of $\dot{\theta}$ in (24a) leads to instability. As shown in Fig. 8, however, decreasing X/R may further lead to shrinking the stable k_p range with a higher k_q . In general, it is more beneficial to properly select the virtual impedance to ensure $X/R > 1$ for further expansion of stability region.

III. GENERALIZED MULTI-TIMESCALE APPROACH

In this section, a formulation of a general method for stability analysis of multiple timescale systems is presented. The method represents a first-order of the, so-called, singular perturbation theory as opposed to zero-order, which corresponds to neglecting the dynamics of fast variables altogether. Employing

this method allows for proper inclusion of possible effect fast variables have on slow modes. The presence of strong timescale separation in microgrids manifests itself in the appearance of several clusters of modes on the plane of system eigenvalues with only one cluster, corresponding to the slowest modes, associated with power controllers, is of interest from the point of view of small-signal stability [22], [32]. Let us start from the general description of a system with a set of first-order differential equations linearized around an equilibrium point:

$$\delta\dot{x} = A\delta x \quad (27)$$

where x is a set of system variables and A is the corresponding Jacobian matrix. It is desirable to aim at such a simplification of a system representation, that only the relevant modes are considered in the form of dynamic equations and all the rest are properly eliminated. The timescale separation was presented in [27] where the authors introduced a two time-scale model of a system and completely excluded the dynamics of “fast” variables by using their quasi-stationary values and considered three different ways of separating the initial set into “fast” and “slow” degrees of freedom. In the present paper, a more systematic procedure of timescale separation will be presented along with a procedure for proper exclusion of fast degrees of freedom while accounting for their effect in the reduced-order system. The separation of the system in (27) into two subsystems corresponding to slow and fast variables gives:

$$\delta\dot{x}_s = A_{ss}\delta x_s + A_{sf}\delta x_f \quad (28)$$

$$\Gamma\delta\dot{x}_f = A_{fs}\delta x_s + A_{ff}\delta x_f \quad (29)$$

where the subscripts s and f correspond to slow and fast degrees of freedom, respectively; Γ is a set of parameters designating fast degrees of freedom. A procedure employed in [27] neglects the left-hand side of (29), thus reducing the system in (28) to the following (see Appendix B for details):

$$\delta\dot{x}_s = (A_{ss} - A_{sf}A_{ff}^{-1}A_{fs})\delta x_s \quad (30)$$

The stability of such a system is certified by demanding all the eigenvalues of the new state matrix $(A_{ss} - A_{sf}A_{ff}^{-1}A_{fs})$ to have negative real parts.

Expression (30) can be treated as a zero's order approximation of the perturbation approach. It is formally obtained by stating a linear relation between δx_f and δx_s which is found from (29) by neglecting its left-hand side (details are provided in Appendix B). Let us now consider the next order by stating that the first derivative of δx_f is non-zero (i.e., $\delta\dot{x}_f \neq 0$), but the second derivative is negligible. Inserting such a dependence in (29) and separating different orders of magnitude, one finds:

$$\delta x_f = -A_{ff}^{-1}A_{fs}\delta x_s - A_{ff}^{-1}\Gamma A_{ff}^{-1}A_{fs}\delta\dot{x}_s \quad (31)$$

Inserting this into (28), the following is obtained:

$$(1 + A_{sf}A_{ff}^{-1}\Gamma A_{ff}^{-1}A_{fs})\delta\dot{x}_s = (A_{ss} - A_{sf}A_{ff}^{-1}A_{fs})\delta x_s \quad (32)$$

which is a generalization of (30) and 1 in the left-hand side of (32) represents a unity matrix. The described procedure is rather general and incorporates the cases when some of the fast

degrees of freedom are “instantaneous” which correspond to respective elements of Γ being zero such that algebraic constraints can also be treated. The convenience of the representation used lies in the fact that one can operate with a general set of fast degrees of freedom without the need to first separate the linearly independent ones or solve for individual variables derivatives.

The general expression (32) can be used in order to explain why the fast degrees of freedom can play an important role in system stability and why using quasi-stationary approximation can be unjustified. The stability of such a system is certified only if the full state matrix $(A_{ss} - A_{sf}A_{ff}^{-1}A_{fs})^{-1}(A_{ss} - A_{sf}A_{ff}^{-1}A_{fs})$ satisfies the Routh-Hurwitz criterion. It is not uncommon that the quasi-stationary state matrix $(A_{ss} - A_{sf}A_{ff}^{-1}A_{fs})$ has all the real parts of its eigenvalues negative, thus certifying the stability of the quasi-stationary system (30) while the full state matrix has positive real parts of one or more of its eigenvalues making the whole system unstable. This is exactly the case with the stability of a droop-controlled inverter connected to an external grid which was considered in details in the previous section.

The influence of fast degrees of freedom is described by the term $A_{sf}A_{ff}^{-1}\Gamma A_{ff}^{-1}A_{fs}$ which is added to a unity matrix. While the timescale parameters Γ can be arbitrarily small, it is not the components of matrix Γ itself that should be compared to unity, but rather the components of the matrix $A_{sf}A_{ff}^{-1}\Gamma A_{ff}^{-1}A_{fs}$ which are not necessarily small. This illustrates why a simple observation of time-scales (looking at components of Γ matrix) of the initial problem can not give a reliable conclusion about the possibility to omit a certain degree of freedom from dynamic equations. One should look at the components of the matrix $A_{sf}A_{ff}^{-1}\Gamma A_{ff}^{-1}A_{fs}$ in order to judge whether the role of fast state is significant or not.

IV. NETWORK GENERALIZATION

A general approach derived in the previous section can be used to derive a reduced-order system of dynamic equations for microgrids with multiple inverters and loads. Formally, the method can be applied to microgrids with arbitrary structure including those containing loads with nontrivial dynamics - at the first step one needs to separate the “slow” and “fast” states and then follow the described procedure to arrive to equations (32). Here, an application of the method to microgrids containing multiple droop-controlled inverters and constant impedance loads will be presented. It is important to note that this procedure can be also directly applied to networks with constant power loads (CPL) and current-controlled inverters, which should be simply treated as constant power sources (CPS). Although the power consumed by CPL or dispatched by CPS can change on larger timescales, for small-signal stability studies it is sufficient to treat them as constant power components by taking a snapshot of operating conditions for a given instant. The influence of power electronics controlled CPL on the stability of inverter-based microgrids has been extensively studied in [36] with the conclusion that there is limited effect from the load dynamics on the power controllers of inverters. Therefore, for the purpose of small-signal stability studies of a microgrid contain-

ing droop-controlled inverters along with non-dispatchable DGs and constant power loads, the two latter components can be effectively substituted by their linearized equivalent impedances. In the following, we use the term “inverter” only in reference to droop-controlled ones, all the remaining components of a microgrid (like current-controlled inverters) are referred to as loads or sources and treated as described above.

Generalization of the proposed model presented in Section II to networks is done directly by constructing a system of dynamic equations similar to (24) for every inverter node. First, a network admittance matrix $\mathbf{Y}(s)$ (in Laplace representation) should be constructed using the full network impedance matrix where all the line and effective load impedances $Z_{ij}(s)$ are written in Laplace domain (i.e., $Z_{ij} = R_{ij} + j\omega_0 L_{ij} + sL_{ij}$). Matrix $\mathbf{Y}(s)$ links inverter voltages to inverter currents:

$$\mathbf{I}(s) = \mathbf{Y}(s)\mathbf{V}(s) \quad (33)$$

where $\mathbf{I}(s)$ and $\mathbf{V}(s)$ are the Laplace transforms of the complex vectors of inverter currents and voltages, respectively. The equivalent network contains inverter buses that are interconnected through lines in addition to shunt elements attached to inverter buses to represent loads. It is convenient to separate the total admittance matrix into the “network” (denoted by index N) and the “load” (denoted by index L) parts:

$$\mathbf{Y}(s) = \mathbf{Y}_N(s) + \mathbf{Y}_L(s) \quad (34)$$

where the “load” admittance matrix $\mathbf{Y}_L(s)$ is diagonal. Then, the next step is to expand the admittance matrix using first-order Taylor expansion:

$$\mathbf{Y}(s) \approx \mathbf{Y}_0 + \mathbf{Y}_1 s \quad (35)$$

where

$$\mathbf{Y}_0 = \mathbf{Y}(s)|_{s=0} \quad (36)$$

$$\mathbf{Y}_1 = \left. \frac{\partial \mathbf{Y}(s)}{\partial s} \right|_{s=0} \quad (37)$$

After substitution in (33) and switching back to time domain, a generalized version of (20) is obtained:

$$\mathbf{I}(t) = [\mathbf{Y}_{0N} + \mathbf{Y}_{0L}] \mathbf{V}(t) + [\mathbf{Y}_{1N} + \mathbf{Y}_{1L}] \dot{\mathbf{V}}(t) \quad (38)$$

One can note that in general it is not appropriate to use the quasi-stationary reduced admittance matrix (\mathbf{Y}_0) for network dynamic simulation, since the proper network representation should be calculated using the initial structure with full impedances (including the Laplace parameter s).

Then, the relations (35) and (38) can be used to construct the generalized dynamic equations of a system with interconnected inverters and loads and, similarly to (24) we get:

$$\tau \mathbf{\Lambda}_p \ddot{\vartheta} + (\mathbf{\Lambda}_p - \mathbf{B}') \dot{\vartheta} + \mathbf{B} \vartheta + (\mathbf{G} + \tilde{\mathbf{G}}) \varrho - \mathbf{G}' \dot{\varrho} = 0 \quad (39a)$$

$$(\tau \mathbf{\Lambda}_q - \mathbf{B}') \dot{\varrho} + (\mathbf{\Lambda}_q + \mathbf{B} + \tilde{\mathbf{B}}) \varrho - \mathbf{G} \vartheta + \mathbf{G}' \dot{\vartheta} = 0 \quad (39b)$$

where ϑ and ϱ are vectors of inverter angles and (relative) voltages, respectively; and all the terms in bold are square matrices with dimensions corresponding to the number of inverters in the grid. $\mathbf{\Lambda}_p$ and $\mathbf{\Lambda}_q$ represent the diagonal matrices with elements

equal to the inverse of frequency and voltage droop coefficients, respectively.

Matrices \mathbf{B} , $\tilde{\mathbf{B}}$, \mathbf{G} and $\tilde{\mathbf{G}}$ can be expressed in terms of the quasi-stationary network admittance matrix:

$$\mathbf{B} = -U_0^2 \text{Im} \{ \mathbf{Y}_{0N} \}, \quad \mathbf{G} = U_0^2 \text{Re} \{ \mathbf{Y}_{0N} \} \quad (40)$$

$$\tilde{\mathbf{B}} = -2U_0^2 \text{Im} \{ \mathbf{Y}_{0L} \}, \quad \tilde{\mathbf{G}} = 2U_0^2 \text{Re} \{ \mathbf{Y}_{0L} \} \quad (41)$$

It is important to note that both \mathbf{B} and \mathbf{G} are singular but positive semi-definite matrices, while $\tilde{\mathbf{B}}$ and $\tilde{\mathbf{G}}$ are diagonal and positive-definite matrices. Matrices \mathbf{B}' and \mathbf{G}' represent the effect of network and load dynamics, and can be expressed in terms of \mathbf{Y}_1 :

$$\mathbf{B}' = U_0^2 \text{Im} \{ \mathbf{Y}_{1N} + \mathbf{Y}_{1L} \} \quad (42a)$$

$$\mathbf{G}' = -U_0^2 \text{Re} \{ \mathbf{Y}_{1N} + \mathbf{Y}_{1L} \} \quad (42b)$$

Since \mathbf{B}' and \mathbf{G}' are obtained from the admittance matrix through linear operation, they preserve the general property: diagonal element is equal to the negative sum of all elements in a corresponding row plus the shunt admittance due to a load attached to the corresponding bus. One can also note that matrix \mathbf{B}' is positive definite, while matrix \mathbf{G}' is sign indefinite. Typically, the equivalent impedances of loads are much larger than the impedances of the lines, so one would expect their effect to be negligible (this is also confirmed in [36] and [37]).

Equations (39) allow one to analyze the stability of a multi-inverter system taking into account the network dynamics, while still having an effective low-order form with simple representation of droop coefficients. The main value of such a representation is that the resulting equations contain only local (i.e., related to a single inverter) dynamic states with all the non-local variables being properly excluded. Such a property of dynamic equations is crucial for development of certain advanced methods for stability assessment [23]–[25], however, as was explicitly pointed out in [28], a simplified representation with network dynamics neglected does not allow for proper assessment of microgrids stability. Therefore, an important contribution of this work is that it introduces a new model for microgrids stability study possessing the simplicity of oscillator-type quasi-stationary reduced-order models but at the same time properly accounting for important network dynamics. Any existing techniques that are known for quasi-stationary approximation can now be directly applied to this model with the network dynamics effects automatically taken into account.

V. NUMERICAL EVALUATION

A. Model Accuracy

In this section, simulation results comparing the different models are presented. To verify the accuracy of the proposed reduced-order model, a system with five inverters in the cascade configuration shown in Fig. 9 is investigated, in which the coupling inductors are included into the network in \mathbf{Y} representation. The system parameters of five inverter-based microgrid are given in Table I in the Appendix. First, a time-domain simulation was conducted to compare the dynamic responses

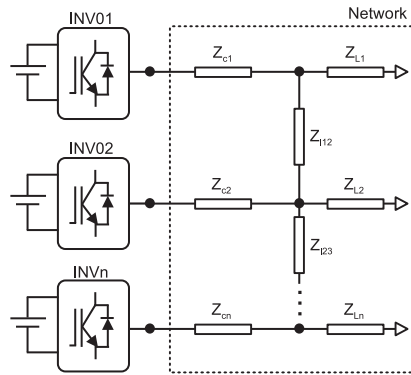


Fig. 9. System configuration of inverter-based microgrid under study.

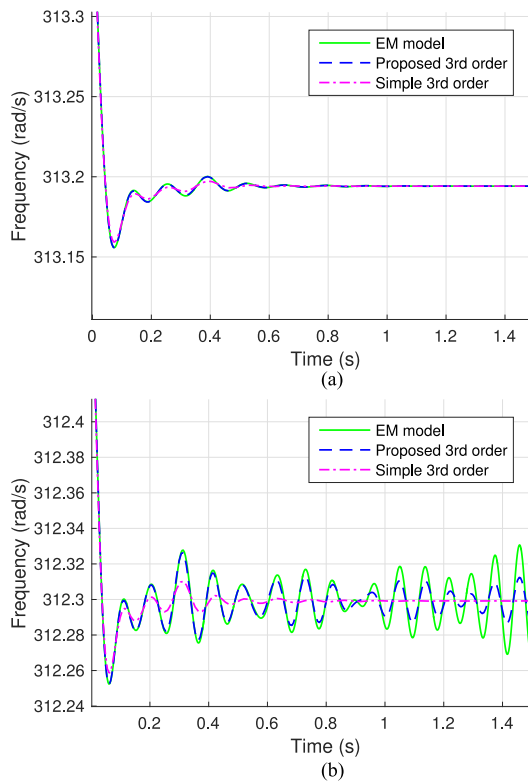


Fig. 10. Dynamic responses of different models with different droop gains. (a) $k_p = 0.45\%$. (b) $k_p = 0.75\%$.

predicted by different models for different values of droop coefficients, as shown in Fig. 10. It is shown that all the models match very well when the operating droop gains are far away from the instability boundary which is shown in Fig. 10(a). The discrepancies between the models become significant when the system reaches instability as shown in Fig. 10(b), where erroneous prediction of stable operation can be observed from the conventional simple 3rd-order model, while the EM and the developed high-fidelity model give correct prediction of the onset of instability. We would like to emphasize that the performance of reduced-order model in dynamic simulations for certain number of operating points is not a sufficient indicator of the model quality - one needs to look at the stability boundaries predicted by the model in order to draw conclu-

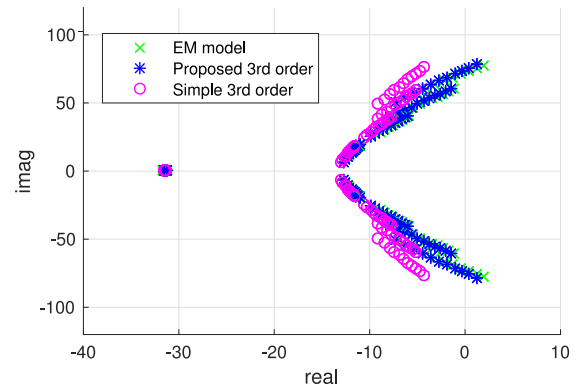


Fig. 11. Eigenvalue plots of different models ($k_p = 0.3\% - 0.75\%$).

sions about its accuracy. Furthermore, a comparison of eigenvalue movements by varying k_p for different models is given in Fig. 11. It can be seen that the eigenvalues of the system calculated using the proposed 3rd-order model are much closer to the EM model as compared to the simple 3rd-order model, which is consistent with the simplified two-bus results presented in Section II.

B. Simulation Efficiency

Another important feature of the proposed reduced-order model is that it mitigates the computation burden on the time-domain simulation. For the EM model, all the cable and load dynamics are modelled as states. The total number of states (n_s) is approximately 9 times the number of inverters in the cascade topology. In comparison, the proposed technique requires only 3 states per inverter, which reduces the number of states by two-thirds. This allows us to handle a network system with a large number of inverters. To identify the efficiency of the proposed model, the EM and proposed 3rd-order models are tested via time-domain simulation with Matlab default O.D.E. solvers. The inverters, coupling inductors, and the lines/cables are assumed to be identical for simplicity. The simulation time is set to be one second. The results are shown in Table II for 5 and 25 inverter-based microgrids. These results clearly demonstrate that the proposed model reduces the number of states and improves the simulation efficiency significantly.

VI. CONCLUSION

Contrary to large-scale power grids, network dynamics of microgrids, despite its faster time-scales, can greatly influence the behavior of slow degrees of freedom associated with inverter power controllers. Particularly, the stability region in terms of voltage and frequency droop coefficients is significantly diminished compared to the one predicted by a simple quasi-stationary model. In this paper, an insight to the physical mechanism of instability is presented along with a method for proper exclusion of fast network degrees of freedom without compromising the accuracy of the model while bringing major simplifications in terms of computational complexity and model transparency. The influence is reflected in the corresponding change of the coefficients of the resulting 3rd-order model compared to a purely

quasi-stationary approximation (neglecting the fast degrees of freedom altogether) which leads to significant changes in the predicted regions of stability. The proposed technique is used to illustrate the microgrid specific effects, namely deterioration of stability by reduction of network impedances and/or inverter ratings. The proposed technique is then generalized to microgrid with multiple inverters and arbitrary network structure where the dynamic equations with only local state variables are derived. Future studies will focus on the development of more advanced stability assessment methods based on the proposed reduced-order model. The method of Lyapunov functions may allow for formulation of stability criteria dealing with each inverter's droop coefficients and connecting lines separately or with pairs of interconnected inverters. Such criteria can be used for assessment of stability during system reconfiguration or multiple microgrid interconnection.

APPENDIX A

Here, we provide the detailed derivation of equation (24). First, let us start from the general expression $P_m + jQ_m = Ue^{j\theta} I^*$. The current phasor approximation is given by (20) with I^0 given by (9). By taking the time derivative, one obtains:

$$I \approx I^0 - \frac{L}{(R + j\omega_0 L)^2} [\dot{U}e^{j\theta} - j\dot{\theta}Ue^{j\theta}] \quad (43)$$

Then, by taking the conjugate of (43) and multiplying by the voltage phasor $Ue^{j\theta}$, one can get:

$$P_m + jQ_m = P_m^0 + jQ_m^0 - \frac{L}{(R - j\omega_0 L)^2} [U\dot{U} + j\dot{\theta}U^2] \quad (44)$$

After separation of the real and imaginary part and setting $U \approx U_b = 1$ pu in the second term in the right-hand side, the expression from (21) is obtained (we also use $\dot{\theta} = \delta\dot{\theta}$, $\dot{U} = \delta\dot{U}$).

APPENDIX B

Here, the detailed derivation of equation (32) is provided. First, let us start from the initial equation for fast states dynamics:

$$\Gamma \delta \dot{x}_f = A_{f_s} \delta x_s + A_{f_f} \delta x_f \quad (45)$$

Then, we seek for δx_f as a series:

$$\delta x_f \approx \delta x_f^{(0)} + \delta x_f^{(1)} + \delta x_f^{(2)} \dots \quad (46)$$

where superscripts in brackets designate the orders of perturbation expansion. For our purposes, we only need the zeros and first order terms. Inserting them into (45) will give:

$$\Gamma \delta \dot{x}_f^{(0)} + \Gamma \delta \dot{x}_f^{(1)} = A_{f_s} \delta x_s + A_{f_f} \delta x_f^{(0)} + A_{f_f} \delta x_f^{(1)} \quad (47)$$

Separating the zero and first order terms (in this respect, the second term in the left-hand side has a second order and should be omitted), one can find:

$$A_{f_s} \delta x_s + A_{f_f} \delta x_f^{(0)} = 0 \quad (48)$$

$$\Gamma \delta \dot{x}_f^{(0)} = A_{f_f} \delta x_f^{(1)} \quad (49)$$

TABLE I
PARAMETERS OF FIVE INVERTER-BASED MICROGRID

Parameter	Description	Value
U_b	Base Peak Phase Voltage	381.58 V
S_b	Base Inverter Apparent Power	10 kVA
ω_0	Nominal Frequency	2×50 rad/s
L_c	Coupling Inductance	0.35 mH
R_c	Coupling Resistance	30 m Ω
w_c	Filter Constant	31.4 rad/s/W
m_p	Default $P - \omega$ Droop Gain	9.3×10^{-5} rad/s/W
n_q	Default $Q - V$ Droop Gain	1.3×10^{-3} V/Var
L_l	Line Inductance	0.26 mHKm $^{-1}$
R_l	Line Resistance	165 m Ω Km $^{-1}$
l_{ij}	Line Length	[5, 4.1, 3, 6] km
Z_1	Bus 1 Load	25 Ω
Z_2	Bus 2 Load	20 Ω
Z_3	Bus 3 Load	20 + 4.72i Ω
Z_4	Bus 4 Load	40 + 12.58i Ω
Z_5	Bus 5 Load	18.4 + 0.157i Ω
X/R	Average X/R Ratio	0.6224

TABLE II
COMPUTATIONAL TIME COMPARISON

	n = 5		n = 25	
	EM	Proposed	EM	Proposed
n_s	42	15	222	75
ode23	NA	0.118 s	NA	0.119 s
ode23s	17.36 s	0.367 s	>20 s	1.727 s
ode23t	0.345 s	0.067 s	0.926 s	0.08 s
ode23tb	0.384 s	0.073 s	1.14 s	0.097 s

Then, the following expressions are obtained:

$$\delta x_f^{(0)} = -A_{f_f}^{-1} A_{f_s} \delta x_s \quad (50)$$

$$\delta x_f^{(1)} = -A_{f_f}^{-1} \Gamma A_{f_f}^{-1} A_{f_s} \delta \dot{x}_s \quad (51)$$

Inserting these expressions into the equations for slow degrees of freedom in (28), one arrives to (32).

REFERENCES

- [1] N. Hatzigiorgiou, H. Asano, R. Iravani, and C. Marnay, "Microgrids," *IEEE Power Energy Mag.*, vol. 5, no. 4, pp. 78–94, Jul./Aug. 2007.
- [2] R. H. Lasseter, "Smart distribution: Coupled microgrids," *Proc. IEEE*, vol. 99, no. 6, pp. 1074–1082, Jun. 2011.
- [3] M. Smith and D. Ton, "Key connections: The US Department of Energy's microgrid initiative," *IEEE Power Energy Mag.*, vol. 11, no. 4, pp. 22–27, Jul./Aug. 2013.
- [4] E. Romero-Cadaval, G. Spagnuolo, L. G. Franquelo, C. A. Ramos-Paja, T. Suntio, and W. M. Xiao, "Grid-connected photovoltaic generation plants: Components and operation," *IEEE Ind. Electron. Mag.*, vol. 7, no. 3, pp. 6–20, Sep. 2013.
- [5] D. E. Olivares *et al.*, "Trends in microgrid control," *IEEE Trans. Smart Grid*, vol. 5, no. 4, pp. 1905–1919, Jul. 2014.
- [6] Y. Zoka, H. Sasaki, N. Yorino, K. Kawahara, and C. C. Liu, "An interaction problem of distributed generators installed in a microgrid," in *Proc. IEEE Int. Conf. Elect. Utility Deregulation, Restruct. Power Technol.*, Apr. 2004, pp. 795–799.
- [7] J. Huang, C. Jiang, and R. Xu, "A review on distributed energy resources and microgrid," *Renew. Sustain. Energy Rev.*, vol. 12, no. 9, pp. 2472–2483, 2008.

- [8] S. Parhizi, H. Lotfi, A. Khodaei, and S. Bahramirad, "State of the art in research on microgrids: A review," *IEEE Access*, vol. 3, pp. 890–925, 2015.
- [9] E. Planas, A. Gil-de Muro, J. Andreu, I. Kortabarria, and I. M. de Alegria, "General aspects, hierarchical controls and droop methods in microgrids: A review," *Renew. Sustain. Energy Rev.*, vol. 17, pp. 147–159, 2013.
- [10] R. Majumder, "Some aspects of stability in microgrids," *IEEE Trans. Power Syst.*, vol. 28, no. 3, pp. 3243–3252, Aug. 2013.
- [11] X. Wang, Y. W. Li, F. Blaabjerg, and P. C. Loh, "Virtual-impedance-based control for voltage-source and current-source converters," *IEEE Trans. Power Electron.*, vol. 30, no. 12, pp. 7019–7037, Dec. 2015.
- [12] M. C. Chandorkar, D. M. Divan, and R. Adapa, "Control of parallel connected inverters in stand-alone ac supply systems," *IEEE Trans. Ind. Appl.*, vol. 29, no. 1, pp. 136–143, Jan./Feb. 1993.
- [13] E. Coelho, P. Cortizo, and P. Garcia, "Small-signal stability for parallel-connected inverters in stand-alone ac supply systems," *IEEE Trans. Ind. Appl.*, vol. 38, no. 2, pp. 533–542, Mar./Apr. 2002.
- [14] J. M. Guerrero, L. G. De Vicuna, J. Matas, M. Castilla, and J. Miret, "A wireless controller to enhance dynamic performance of parallel inverters in distributed generation systems," *IEEE Trans. Power Electron.*, vol. 19, no. 5, pp. 1205–1213, Sep. 2004.
- [15] N. Hatziaziyriou, *Microgrids: Architectures and Control*. Hoboken, NJ, USA: Wiley, 2013.
- [16] J. He, Y. W. Li, J. M. Guerrero, F. Blaabjerg, and J. C. Vasquez, "An islanding microgrid power sharing approach using enhanced virtual impedance control scheme," *IEEE Trans. Power Electron.*, vol. 28, no. 11, pp. 5272–5282, Nov. 2013.
- [17] J. He and Y. W. Li, "Analysis, design, and implementation of virtual impedance for power electronics interfaced distributed generation," *IEEE Trans. Ind. Appl.*, vol. 47, no. 6, pp. 2525–2538, Nov. 2011.
- [18] W. Yao, M. Chen, J. Matas, J. M. Guerrero, and Z.-M. Qian, "Design and analysis of the droop control method for parallel inverters considering the impact of the complex impedance on the power sharing," *IEEE Trans. Ind. Electron.*, vol. 58, no. 2, pp. 576–588, Feb. 2011.
- [19] J. M. Guerrero, J. C. Vasquez, J. Matas, L. G. De Vicuña, and M. Castilla, "Hierarchical control of droop-controlled ac and dc microgrids—A general approach toward standardization," *IEEE Trans. Ind. Electron.*, vol. 58, no. 1, pp. 158–172, Jan. 2011.
- [20] J. Kim, J. M. Guerrero, P. Rodriguez, R. Teodorescu, and K. Nam, "Mode adaptive droop control with virtual output impedances for an inverter-based flexible ac microgrid," *IEEE Trans. Power Electron.*, vol. 26, no. 3, pp. 689–701, Mar. 2011.
- [21] J. M. Guerrero, M. Chandorkar, T.-L. Lee, and P. C. Loh, "Advanced control architectures for intelligent microgrids—Part i: Decentralized and hierarchical control," *IEEE Trans. Ind. Electron.*, vol. 60, no. 4, pp. 1254–1262, Apr. 2013.
- [22] N. Pogaku, M. Prodanović, and T. C. Green, "Modeling, analysis and testing of autonomous operation of an inverter-based microgrid," *IEEE Trans. Power Electron.*, vol. 22, no. 2, pp. 613–625, Mar. 2007.
- [23] J. W. Simpson-Porco, F. Dörfler, and F. Bullo, "Droop-controlled inverters are kuramoto oscillators," *IFAC Proc. Volumes*, vol. 45, no. 26, pp. 264–269, 2012.
- [24] Y. Zhang, L. Xie, and Q. Ding, "Interactive control of coupled microgrids for guaranteed system-wide small signal stability," *IEEE Trans. Smart Grid*, vol. 7, no. 2, pp. 1088–1096, Mar. 2016.
- [25] Y. Zhang and L. Xie, "Online dynamic security assessment of microgrid interconnections in smart distribution systems," *IEEE Trans. Power Syst.*, vol. 30, no. 6, pp. 3246–3254, Nov. 2015.
- [26] L. Luo and S. V. Dhople, "Spatiotemporal model reduction of inverter-based islanded microgrids," *IEEE Trans. Energy Convers.*, vol. 29, no. 4, pp. 823–832, Dec. 2014.
- [27] I. P. Nikolakakos, H. H. Zeineldin, M. S. El-Moursi, and N. D. Hatziaziyriou, "Stability evaluation of interconnected multi-inverter microgrids through critical clusters," *IEEE Trans. Power Syst.*, vol. 31, no. 4, pp. 3060–3072, Jul. 2016.
- [28] V. Mariani, F. Vasca, J. C. Vásquez, and J. M. Guerrero, "Model order reductions for stability analysis of islanded microgrids with droop control," *IEEE Trans. Ind. Electron.*, vol. 62, no. 7, pp. 4344–4354, Jul. 2015.
- [29] S. V. Iyer, M. N. Belur, and M. C. Chandorkar, "A generalized computational method to determine stability of a multi-inverter microgrid," *IEEE Trans. Power Electron.*, vol. 25, no. 9, pp. 2420–2432, Sep. 2010.
- [30] X. Guo, Z. Lu, B. Wang, X. Sun, L. Wang, and J. M. Guerrero, "Dynamic phasors-based modeling and stability analysis of droop-controlled inverters for microgrid applications," *IEEE Trans. Smart Grid*, vol. 5, no. 6, pp. 2980–2987, Nov. 2014.
- [31] M. Rasheduzzaman, J. A. Mueller, and J. W. Kimball, "Reduced-order small-signal model of microgrid systems," *IEEE Trans. Sustain. Energy*, vol. 6, no. 4, pp. 1292–1305, Oct. 2015.
- [32] Y. A.-R. I. Mohamed and E. F. El-Saadany, "Adaptive decentralized droop controller to preserve power sharing stability of paralleled inverters in distributed generation microgrids," *IEEE Trans. Power Electron.*, vol. 23, no. 6, pp. 2806–2816, Nov. 2008.
- [33] J. Machowski, J. Bialek, and J. Bumby, *Power System Dynamics: Stability and Control*. Hoboken, NJ, USA: Wiley, 2011.
- [34] J. M. Guerrero, L. G. de Vicuna, J. Matas, M. Castilla, and J. Miret, "Output impedance design of parallel-connected ups inverters with wireless load-sharing control," *IEEE Trans. Ind. Electron.*, vol. 52, no. 4, pp. 1126–1135, Aug. 2005.
- [35] Q. C. Zhong and G. Weiss, "Synchronverters: Inverters that mimic synchronous generators," *IEEE Trans. Ind. Electron.*, vol. 58, no. 4, pp. 1259–1267, Apr. 2011.
- [36] N. Bottrell, M. Prodanovic, and T. C. Green, "Dynamic stability of a microgrid with an active load," *IEEE Trans. Power Electron.*, vol. 28, no. 11, pp. 5107–5119, Nov. 2013.
- [37] N. Jayawarna, X. Wu, Y. Zhang, N. Jenkins, and M. Barnes, "Stability of a microgrid," in *Proc. 3rd IET Int. Conf. Power Electron., Mach. Drives*, 2006, pp. 316–320.



Petr Vorobev (M'15) received the Ph.D. degree in theoretical physics from Landau Institute for Theoretical Physics, Moscow, Russia, in 2010. He is currently a Postdoctoral Associate in the Mechanical Engineering Department, Massachusetts Institute of Technology (MIT), Cambridge, MA, USA. His research interests include a broad range of topics related to power system dynamics and control. This covers low-frequency oscillations in power systems, dynamics of power system components, multi-timescale approaches to power system modeling, and development of plug-and-play control architectures for microgrids.



Po-Hsu Huang (SM'12) received the B.Sc. degree from National Cheng-Kung University, Tainan, Taiwan, and the first M.Sc. degree from National Taiwan University, Taipei, Taiwan, in 2007 and 2009, respectively, both in electrical engineering, and the second M.Sc. degree from the Department of Electrical Power Engineering, Masdar Institute of Science and Technology, Abu Dhabi, UAE. He is currently working toward the Ph.D. degree in the Department of Electrical Engineering and Computer Science, Massachusetts Institute of Technology, Cambridge, MA, USA. His current interests include photovoltaic power systems, DC/AC microgrids, power electronics, wind power generation, linear/nonlinear system dynamics, power system stability, and control.



Mohamed Al Hosani (S'10–M'13) received the B.Sc. degree in electrical engineering from the American University of Sharjah, Sharjah, UAE, in 2008, and the M.Sc. and the Ph.D. degrees in electrical engineering from the University of Central Florida, Orlando, FL, USA, in 2010 and 2013, respectively. Since 2014, he has been with the Department of Electrical Engineering and Computer Science, Masdar Institute of Science and Technology, Abu Dhabi, UAE, as an Assistant Professor. He was a Visiting Assistant Professor at the Massachusetts Institute of Technology, Cambridge, MA, USA, for 8 months during 2015–2016. His current interests include anti-islanding algorithm, distributed generation protection and control, and modeling and stability analysis of micro-grid and smart grid.



James L. Kirtley, Jr. (F'90-LF'11) received the Ph.D. degree from Massachusetts Institute of Technology, Cambridge, MA, USA, in 1971. He is a Professor of Electrical Engineering at the Massachusetts Institute of Technology. He was with General Electric, Large Steam Turbine Generator Department, as an Electrical Engineer, for Satcon Technology Corporation as the Vice President and General Manager of the Tech Center, and as a Chief Scientist and Director. He was Gastdozent at the Swiss Federal Institute of Technology. He is a specialist in electric machinery and electric power systems.

He served as the Editor-in-Chief of the IEEE TRANSACTIONS ON ENERGY CONVERSION from 1998 to 2006 and continues to serve as an Editor for that journal and as a member of the Editorial Board of the journal *Electric Power Components and Systems*. He received the IEEE Third Millennium medal in 2000 and the Nikola Tesla prize in 2002. He was elected to the United States National Academy of Engineering in 2007. He is a Registered Professional Engineer in Massachusetts.



Konstantin Turitsyn (M'09) received the M.Sc. degree in physics from Moscow Institute of Physics and Technology, Dolgoprudny, Russia, and the Ph.D. degree in physics from Landau Institute for Theoretical Physics, Moscow, Russia, in 2007. He is currently an Assistant Professor in the Mechanical Engineering Department, Massachusetts Institute of Technology (MIT), Cambridge, MA, USA. Before joining MIT, he held the position of an Oppenheimer Fellow at Los Alamos National Laboratory, USA, and a KadanoffRice Postdoctoral Scholar at the University

of Chicago, Chicago, IL, USA. His research interests include a broad range of problems involving nonlinear and stochastic dynamics of complex systems. Specific interests in energy-related fields include stability and security assessment, integration of distributed and renewable generation.